PAPER Nr.: 96

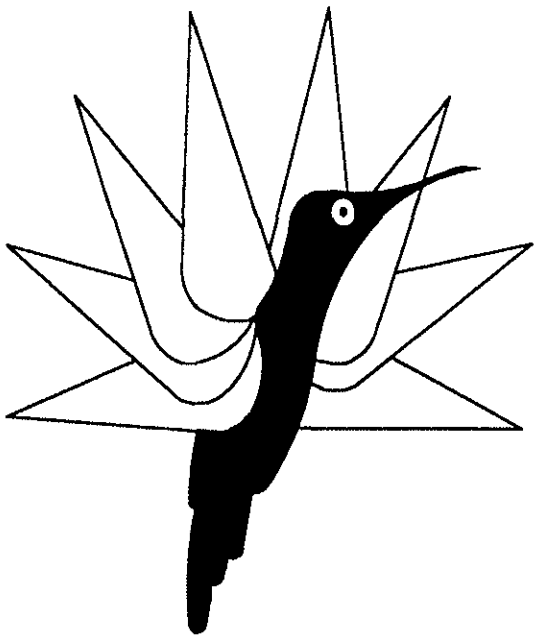

AEROELASTIC OPTIMIZATION OF AN ADVANCED GEOMETRY HELICOPTER ROTOR WITH COMPOSITE TAILORING

BY

RANJAN GANGULI AND INDERJIT CHOPRA

CENTER FOR ROTORCRAFT EDUCATION AND RESEARCH
DEPARTMENT OF AEROSPACE ENGINEERING
UNIVERSITY OF MARYLAND AT COLLEGE PARK, MARYLAND 20742, USA

TWENTIETH EUROPEAN ROTORCRAFT FORUM
OCTOBER 4 - 7, 1994 AMSTERDAM

Printed by the Technical Highschool Haarlem

AEROELASTIC OPTIMIZATION OF AN ADVANCED GEOMETRY HELICOPTER ROTOR WITH COMPOSITE TAILORING

Ranjan Ganguli * Inderjit Chopra †

Center for Rotorcraft Education and Research
Department of Aerospace Engineering
University of Maryland at College Park, Maryland 20742, USA.

ABSTRACT - An aeroelastic analysis based on a finite element method in space and time is developed for an advanced geometry rotor with multi-cell composite cross-sections. Sensitivity analysis is performed using an analytical approach. Optimization studies are carried out for a four-bladed, soft-inplane advanced geometry composite rotor consisting of a variable sweep, anhedral and planform taper, and with a two-cell box-beam spar. The objective function includes vibratory hub loads and vibratory bending moments; constraints are imposed on blade rotating frequencies, aeroelastic stability and autorotational inertia. Design variables include ply angles of the laminated walls of the box-beam, sweep, droop and planform taper, and nonstructural mass and its chordwise offset from the elastic axis. Aeroelastic optimization is performed for different combinations of design variables. The starting design is a straight blade with no composite coupling. Compared to the starting design, an optimized solution achieved a reduction in the 4/rev loads of 40-60 percent, and 17 and 26 percent, respectively, in the peak-to-peak vibratory flap and lag bending moments.

NOMENCLATURE

c	blade chord	c_{tp}	planform taper
$\mathbf{C}$	modal damping matrix	$\mathbf{D}$	design variables D_j, $j = 1, \ldots n$
EI_y	blade flap bending stiffness	EI_z	blade lag bending stiffness
$\mathbf{F}$	modal force vector	GJ	blade torsional stiffness
J	objective function	k_A	radius of gyration of blade cross section
$\mathbf{K}$	modal stiffness matrix	$\mathbf{K}^s$	structural stiffness matrix
$\mathbf{K}_t$	tangential stiffness matrix	m_{ns}	nonstructural mass
m_0	reference mass per unit length	$\mathbf{M}$	modal mass matrix
$\mathbf{M}^s$	structural mass matrix	$\mathbf{Q}$	state variable of load vectors
$\mathbf{q}$	blade global coordinates	R	rotor radius
y_{ns}	chordwise offset of nonstructural mass from elastic axis (positive forward)	$\mathbf{Y}$	blade response
α_k	real part of characteristic exponent of kth mode	λ_k	eigenvalue of kth stability mode
Λ_1	tip sweep angle (positive forward)	Λ_2	tip anhedral angle (positive upward)
$\tilde{\Lambda}_k$	advanced geometry local-global transformation for kth element	Λ'_k	advanced geometry transformation for kth segment
Φ	mode shape	Ψ	state transition matrix

1. INTRODUCTION

Advanced geometry rotor blades involve variable sweep, anhedral, pretwist and planform taper along the blade length. Such blades are receiving increasing attention from rotor designers seeking to reduce compressibility drag rise, stall effects and acoustic noise. The application of composite materials has made fabrication of such complex geometry rotors feasible. Composite materials offer other advantages over metals such as superior fatigue characteristics, higher stiffness-weight ratio and flexibility in tailoring

*Research Associate

†Professor and Director

Presented as paper No. 96, 20th European Rotorcraft Forum, Amsterdam, The Netherlands, 4-7 October 1994.

structural characteristics, which can be exploited by the rotorcraft industry. Recent research has shown that reduced vibratory hub loads can be obtained by tailoring the blade geometry [1]-[6] as well as by the use of composite tailoring [7]-[15]. The objective of this paper is to apply an optimization methodology to minimize vibration and blade dynamic stresses for helicopters with advanced geometry composite rotor blades having generic, multi-cell cross sections.

Helicopters are susceptible to high vibrations and high blade dynamic stresses due to harmonic loading on the rotor caused by an unsteady aerodynamic environment and highly flexible rotating blades. For example, for a rotor with N blades, the N/rev forces and moments are transmitted by the rotor to the fuselage as a primary source of vibration. A direct approach for reducing helicopter vibration is to design the rotor so as to minimize the vibratory hub loads . The rotor blade is subjected to dynamic stresses at several harmonics caused by the vibratory bending and torsional moments acting along the blade span. These dynamic stresses cause structural fatigue, leading to a reduction in blade life. The critical dynamic stresses generally occur at the spanwise location where the bending moment is highest; for hingeless rotors this occurs at the blade root and for articulated rotors around the blade mid-section. Therefore, a direct approach for increasing the life of a blade is to design the rotor low vibratory bending and torsional moments at the critical spanwise locations.

Over the past few years, considerable research has been directed towards the application of aeroelastic optimization methodology to design rotors with low vibration [16]. That research ranges from simple analyses neglecting aeroelastic coupling to comprehensive studies using refined aeroelastic and sensitivity analyses. The complexity and computational expense associated with aeroelastic optimization has led some researchers to formulate simpler strategies for vibration reduction in helicopters, such as blade rotating frequency placement and modal based vibration methods. However, it has been shown that frequency placement is not a reliable means for obtaining vibration reduction [17]. On the other hand, minimization of modal vibration indices and modal hub shears lead to a reduction in the vibratory hub loads; this result has also been verified by wind-tunnel tests comparing a baseline rotor to the optimum rotor [17, 18]. Though these limited experimental testing of optimized rotors based on vibration indices showed potential for vibration reduction, the lack of aeroelastic couplings in the analysis may lead to erroneous conclusions. Modal based optimization methods are computationally inexpensive and easy to implement but often neglect the aeroelastic interactions (between the airloads and the blade response).

The assumptions involved in modal based optimization can be avoided by using an optimization procedure based on a comprehensive aeroelastic analysis. The use of such optimization algorithms requires calculation of the gradient of the objective function and constraints. These gradients are needed to determine the search direction along which the objective function decreases without violating the constraints. Most of the studies on aeroelastic optimization of helicopter rotors use finite difference methods for calculating these gradients. Because of large computer time requirements, such studies are restrictive in terms of the objective function, constraints and design variables. In order to reduce computer time, some researchers have used analytical methods [13]-[15], [19] to calculate the gradients. Some other researchers have focused on more efficient optimization techniques such as 'approximation methods' where the computationally expensive aeroelastic optimization problem is replaced by a sequence of approximate problems using Taylor's series expansions [1]. These approximate problems can be solved using much less computer time.

Most studies on aeroelastic optimization of helicopter rotors have been conducted using straight metal blades. Typically, the objective is to minimize vibratory loads acting on the helicopter in forward flight while keeping the blade aeroelastically stable. Selected attempts have been made to perform aeroelastic optimization of straight composite blades and swept-tip metal blades.

For performing aeroelastic optimization of composite blades, an accurate aeroelastic analysis in forward flight is the first necessary step. Over the past few years, there have been attempts to analyze stability and response of straight composite rotors with structural coupling [9]-[12]. Recently, authors [13]-[14] also developed a formulation to carry out aeroelastic optimization of composite rotor blades. The comprehensive aeroelastic code UMARC [20] was modified to include calculation of sensitivity derivatives of a composite rotor using an analytical scheme. The design sensitivity analysis was implemented as an integral part of the blade response and stability analysis and then coupled with the optimizer CONMIN [21]. Numerical results were obtained for a four-bladed, soft-inplane, hingeless composite rotor. The objective was to minimize vibratory hub loads acting on the helicopter in forward flight ($\mu = 0.3$) while keeping the blade aeroelastically stable. The blade spars were modeled as box-beams and the ply angles of the walls of the box-beam were used as design variables. In the first study

[13], authors modeled the blade spar as a single-cell composite box-beam. Section properties for the box-beam were calculated using a composite box-beam analysis [22]. The rotor blade was divided into five spatial finite elements, each having nineteen degrees of freedom (including four shear degrees of freedom). Results of this paper showed that a considerable increase in blade lag mode damping and a measurable decrease in vibratory hub loads can be obtained by tailoring direct stiffnesses and structural coupling. Subsequently, authors [14] modified the aeroelastic optimization analysis of a composite rotor to cover generic multi-cell cross-sections. At the element level, shear degree of freedom were eliminated using static condensation. This procedure allowed the use of the fifteen degrees of freedom finite element similar to that used for metal rotor blades. For numerical studies, the blade spar was modeled as a single-cell and two-cell box beam and section properties of the box-beams were calculated using an extended Vlasov theory [28]. A comparison study showed the validity of using static condensation for rotor aeroelastic, sensitivity and optimization analyses. Results from this optimization study showed enhancement of blade stability and reduction in vibratory loads due to composite tailoring, both at the design condition (μ =0.3) as well as at off-design conditions. However, it was found that the reduction in the 4/rev loads in the fixed frame came at the expense of an increase in the rotating frame loads which are not covered by the objective function (such as 1/rev, 2/rev, 6/rev harmonics), leading to higher dynamic stresses for the optimized blade. Subsequently, a multi-objective optimization study with both vibratory hub loads as well as vibratory bending moments as objective functions was carried out [15]. Using suitable weighting factors, it was shown that it is possible to reduce both the objective functions simultaneously.

Selected studies have been conducted on aeroelastic optimization of swept-tip metal blades. A prerequisite of performing such optimization studies is the availability of accurate aeroelastic analysis. Over the past few years, aeroelastic analyses of swept-tip metal blades have been developed by some researchers [3]-[6].

Celi and Friedmann [1] used a Taylor's series approximation for the objective function and constraints [23] and the approximation technique of Vanderplatts [24] to calculate gradients. They carried out a comprehensive optimization study to minimize oscillatory vertical hub shear for a hingeless rotor with both straight and swept tips, while imposing constraints on frequency placements and blade stability in hover. A reduction of $20-50$ percent in vertical hub shear was obtained. The use of tip sweep as a design variable gave an additional reduction of about 10 percent of vertical hub shear.

Recently, authors [25] carried out an optimization study to minimize the vibratory hub loads of a four-bladed advanced geometry hingeless rotor in forward flight. Constraints included aeroelastic stability, frequency placement and autorotational inertia. The design variables included spanwise variation of blade stiffness and mass properties as well as sweep, droop and planform taper. Results showed a reduction of 25-60 percent in all the 4/rev hub loads.

It is now well established that an advanced geometry blade tip and composite couplings can have considerable influence on blade dynamics. A prerequisite for performing aeroelastic optimization of an advanced geometry composite blade is the availability of an accurate aeroelastic model. Yuan, Friedmann and Venkatesan [26] developed an aeroelastic analysis for swept tip composite rotors. For the present study, a more general aeroelastic analysis for an advanced geometry rotor involving variable sweep, anhedral and planform taper is developed. For this, previous work on composite blades [14] and advanced geometry blades [6] are combined to formulate an aeroelastic analysis for advanced geometry composite blades. This analysis has been implemented in UMARC and the natural frequencies predicted by this analysis have been validated with experimental data [27]. Analytical sensitivity derivatives are calculated as an integral part of the basic aeroelastic analysis and are coupled with the optimization algorithm CONMIN [21] to carry out optimization studies. Results are obtained for different sets of design variables to study the influence of composite couplings and blade geometry on the optimum design.

2. FORMULATION

An advanced geometry rotor aeroelastic analysis, capable of modeling blades with generic composite cross-sections is developed and implemented into UMARC. Key features of this analysis are: (1) use of static condensation to eliminate shear degrees of freedom (2) use of a refined composite beam analysis based on Vlasov theory to calculate section properties of generic multi-cell cross-sections and (3) development of an aeroelastic formulation to allow complete structural coupling between the extension

(u_e), lag bending (v_b), flap bending (w_b) and twist (ϕ) deformations and (4) spanwise variation of sweep, droop and planform taper along the blade length.

The analysis can be divided into two parts. The first part involves the calculation of section properties of a composite beam with multi-cell cross-sections. In the second part, these section properties are used for the aeroelastic analysis of an advanced geometry rotor.

Composite Beam Analysis

Static condensation is used to eliminate shear related degrees of freedom from the composite beam analysis for generic sections developed by Chandra and Chopra [28]. Using this analysis, the static structural equations for an arbitrary cross-section can be written as

$$\begin{Bmatrix} Q_x \\ M_z \\ -M_y \\ M_\omega \\ M_x \\ G_x \\ G_y \\ F_x \\ F_y \end{Bmatrix} = \mathbf{K} \begin{Bmatrix} u_e' \\ v_b'' \\ w_b'' \\ \phi_z'' \\ \phi_z' \\ \epsilon_{xz} \\ \epsilon_{yz} \\ \epsilon_{xz}' \\ \epsilon_{yz}' \end{Bmatrix} \tag{1}$$

The coefficients k_{ij} of the stiffness matrix $\mathbf{K}$ are contour integrals over the cross-section [28]. The axial, flap, lag and torsion deformations are defined by u_e, w_b, v_b and ϕ, respectively and the transverse shears are defined as ϵ_{xz} and ϵ_{yz}. The forces Q_x, M_x, M_z and M_y are associated with the axial, torsion, lag and flap deformations and the shear forces G_x, G_y, F_x and F_y are associated with the shear deformations. The term M_ω is the restrained warping moment and is referred to as the Vlasov torsion. This term becomes important for open section beams where warping restraint effects are important. In the present analysis, this term is set to zero and the effect of restrained warping associated with Vlasov torsion is modeled by modifying the torsional stiffness, K_{55}, along the length of the beam [29]. The shear degrees of freedom are eliminated using static condensation. This is performed in three steps. First, the stiffness matrix defined in Eq. 1 is inverted. Next, from the inverted matrix, the rows and columns corresponding to the shear degrees of freedom and Vlasov torsion are deleted. Finally, the resulting 4×4 matrix is again inverted to give a modified stiffness matrix which implicitly captures the effects of shear. After static condensation, the relations between the generalized forces and displacements can be written as

$$\begin{bmatrix} Q_x \\ M_x \\ -M_y \\ M_z \end{bmatrix} = \begin{bmatrix} \bar{k}_{11} & \bar{k}_{12} & \bar{k}_{13} & \bar{k}_{14} \\ \bar{k}_{12} & \bar{k}_{22} & \bar{k}_{23} & \bar{k}_{24} \\ \bar{k}_{13} & \bar{k}_{23} & \bar{k}_{33} & \bar{k}_{34} \\ \bar{k}_{14} & \bar{k}_{24} & \bar{k}_{34} & \bar{k}_{44} \end{bmatrix} \begin{bmatrix} u_e' \\ \phi' \\ w_b'' \\ v_b'' \end{bmatrix} \tag{2}$$

For an isotropic blade, the off-diagonal terms in the stiffness matrix are zero. Coupled composite blades have non-zero off-diagonal terms.

Aeroelastic Analysis

The advanced geometry blade is modeled using an arbitrary number of Euler-Bernoulli beam type segments, each oriented in space with different sweep, droop and planform taper. The blade can undergo flap bending, lag bending, elastic twist and axial deformation. The formulation also covers chordwise offsets of blade section center of mass, tension center and aerodynamic center from the elastic axis. Each blade segment is modeled using one or more finite elements and intersegment compatibility relations are satisfied using nonlinear transformations [8].

The finite element analysis of the rotor blade is based on Hamilton's principle, which can be written as

$$\delta\Pi = \int_{t_1}^{t_2} (\delta U - \delta T - \delta W) dt = 0 \tag{3}$$

where δU, δT and δW are the virtual strain energy, virtual kinetic energy and virtual work of the system, respectively. The effect of composite materials comes enters in the virtual strain energy, δU; expressions for δT and δW are the same for advanced geometry metal blades and advanced geometry composite blades. These expressions are long and cumbersome and can be found in Ref. 23. Because of involved interelement transformations with sweep, droop, pretwist and time dependent pitch-control, the resulting expressions are significantly more involved compared to those for a straight blade.

Discretization of the Hamilton's principle yields,

$$\delta\Pi = \int_{\psi_i}^{\psi_f} \sum_{i=1}^{N} (\delta U_i - \delta T_i - \delta W_i) d\psi = 0 \tag{4}$$

where δU_i, δT_i and δW_i are the elemental virtual energy contributions and N is the number of beam spatial finite elements. A finite element with fifteen degrees of freedom is used. The aeroelastic analysis involves the calculation of vehicle trim, steady blade response and stability of the rotor perturbation motion. The steady periodic blade response is calculated using a finite element method in time after the nonlinear blade equations in space are transformed into normal mode equations. The nonlinear vehicle trim and blade response equations are solved iteratively as a coupled solution. The linearized periodic rotor perturbation equations are solved using Floquet transition matrix theory. More details on the aeroelastic analysis are available in Ref. [30].

Optimization Analysis

The above aeroelastic and sensitivity analyses of composite rotor blades with generic multi-cell cross-sections are used to conduct aeroelastic optimization.

Objective Function: For the optimization study, three different objective functions are used. The first represents the vibratory hub loads (J_v) alone, the second represents the vibratory blade bending and torsional moments (J_d) and the third represents a combination of both the vibratory hub loads and blade bending moments (J).

The first objective function (J_v) is a sum of the scalar norms of the N/rev forces and the N/rev moments transmitted by an N-bladed helicopter rotor to the fuselage as a primary source of vibration and is defined as

$$J_v = \sqrt{(F_{xH}^{4P})^2 + (F_{yH}^{4P})^2 + (F_{zH}^{4P})^2} + \sqrt{(M_{xH}^{4P})^2 + (M_{yH}^{4P})^2 + (M_{zH}^{4P})^2} \tag{5}$$

where the forces and moments are nondimensionalized with respect to $m_0\Omega^2R^2$ and $m_0\Omega^2R^3$, respectively. Since the forces and moments are of similar magnitude, they are weighted equally in the above objective function.

The second objective function (J_d) is a measure of the vibratory bending and torsional moments at the blade root that are the source of dynamic stresses for a hingeless rotor and is defined as

$$J_d = \sum_{j=1}^{M} j\sqrt{(M_{xR}^{jP})^2 + (M_{yR}^{jP})^2 + (M_{zR}^{jP})^2} \tag{6}$$

Again, the vibratory bending moments in J_d are nondimensionalized by dividing by $m_0\Omega^2R^3$. This function is the weighted norm of the first M harmonics of the blade root bending and torsional moments. The number M is selected depending on the magnitudes of the various harmonics. In general, the 1/rev bending moment is the largest in magnitude and the magnitude of higher harmonic components become much smaller with increasing harmonics. To increase the weight of the higher harmonics (2/rev, 3/rev ,..., M/rev) in the objective function J_d, the j th harmonic component of the objective is multiplied by the number j.

For combined optimization, a weighted objective function J is defined as

$$J = K_1 J_v + K_2 J_d \tag{7}$$

Defining $K_1 + K_2 = 1$, we observe that when $K_1 = 0$, $J = J_d$ and when $K_2 = 0$, $J = J_v$. To give equal weight to both components of the objective function, K_1 and K_2 are chosen by solving the following

equations: $K_1 J_v = K_2 J_d$ and $K_1 + K_2 = 1$. These two equations ensure equal weights for the values of the two components of the objective function. Solving these equations, and substituting the weights K_1 and K_2 in Eq. 7 yields the multicriteria objective function as:

$$J = \frac{2 J_v J_d}{J_v + J_d} \tag{8}$$

Behavior Constraints

The behavior constraints considered in this study are: (1) blade aeroelastic stability and (2) frequency placement and (3) autorotational inertia. The aeroelastic stability constraint keeps the rotor blade stable at a particular flight condition and can be expressed as

$$g_s(D_j) = \alpha_k + \epsilon_k \leq 0, \quad k = 1, \ldots, m \tag{9}$$

where ϵ_k defines the minimum acceptable level of damping (positive for stability) and

$$\alpha_k = \frac{1}{2\pi} ln \sqrt{(\lambda_k^R)^2 + (\lambda_k^I)^2} \tag{10}$$

The λ_k^R and λ_k^I are the real and imaginary parts of the kth eigenvalue λ_k of the Floquet transition matrix at the end of one time period and are calculated by solving the following complex eigenvalue problem:

$$\lambda \mathbf{x} = \Psi(\psi_0 + T, \psi_0)\mathbf{x} \tag{11}$$

where $\Psi(\psi_0 + T, \psi_0)$ is the transition matrix at the end of one time period ($T = 2\pi$), ψ_0 is the initial time, λ is the complex eigenvalue, and $\mathbf{x}$ is the normalized complex eigenvector.

The frequency placement constraint prevents blade resonance at frequencies not covered by the objective function. The frequency constraint for the kth mode can be expressed as

$$g_f^L(D_j) = 1 - \frac{\omega_k}{\omega_k^L} \leq 0 \qquad g_f^U(D_j) = 1 - \frac{\omega_k}{\omega_k^U} \geq 0 \tag{12}$$

where ω_k is the blade rotating natural frequency obtained from the solution of the structural equations:

$$\mathbf{K}^s \Phi = \omega_k^2 \, \mathbf{M}^s \Phi \tag{13}$$

Superscripts L and U denote lower and upper bounds, $\mathbf{K}^s$ and $\mathbf{M}^s$ are the structural stiffness and mass matrices and Φ is the eigenvector.

The autorotation constraint ensures that the rotor has sufficient inertia for safe autorotation.

$$g_a(\mathbf{D}) = R_a - \frac{I}{I_b} \tag{14}$$

The minimum allowable ratio of the blade moment of inertia (I) to the baseline value (I_b) is given by R_a.

Design Variables

The design variables used in this study are the ply angles of the walls of the two-cell box-beam spar (Fig. 1), nonstructural mass and its offset from the elastic axis, and sweep, droop and planform taper. The rotor blade is divided into five spanwise finite elements and the design variables are allowed to vary for different elements. This allows for variation of elastic stiffness and composite coupling along the blade span.

Sensitivity Analysis

The sensitivity derivatives of the objective function and behavior constraints are required by the optimization algorithms. Consider a general function F, which could be the objective function (J), the frequency constraints (g_f) or the stability constraints (g_s). Since F is a function of both the design variables(X_j, θ_i) and the blade response (Y), differentiating F with respect to the design variable X_j and applying chain rule differentiation yields,

$$\frac{dF}{dX_j} = \frac{\partial F}{\partial X_j} + \frac{\partial F}{\partial Y}\frac{\partial Y}{\partial X_j}; \qquad X_j = \lfloor m_{ns}, y_{ns}, \Lambda_1, \Lambda_2, c_{tp} \rfloor \tag{15}$$

X_j are the advanced geometry design variables. The derivatives $\partial F/\partial X_j$ are calculated as an integral part of the aeroelastic analysis using a direct analytical approach. The sensitivity derivatives with respect to the ply angle design variable θ_i are calculated using

$$\frac{dF}{d\theta_i} = \left(\frac{\partial F}{\partial C_j} + \frac{\partial F}{\partial Y}\frac{\partial Y}{\partial C_j}\right)\frac{\partial C_j}{\partial \theta_i} \tag{16}$$

where

$$C_j = \lfloor \bar{k}_{11}, \bar{k}_{12}, \bar{k}_{13}, \bar{k}_{14}, \bar{k}_{22}, \bar{k}_{23}, \bar{k}_{24}, \bar{k}_{33}, \bar{k}_{34}, \bar{k}_{44}, EC_1, EC_2, EB_1, EB_2 \rfloor \tag{17}$$

are the section properties and include all the stiffness and coupling constants contained in the virtual strain energy. Since the computational effort involved with the calculation of section properties of a composite blade is very small, it is convenient to use finite difference approximations to calculate the derivatives $\partial C_j/\partial \theta_i$. The derivatives $\partial F/\partial C_j$ are calculated as an integral part of the aeroelastic analysis using a direct analytical approach.

From the above discussion, it is clear that sensitivity derivatives of F are required with respect to parameters $D_j = \lfloor X_j, C_j \rfloor$. Derivatives of blade response, hub loads, rotating frequency and aeroelastic stability are calculated using an analytical approach as discussed in Ref. 2.

3. RESULTS AND DISCUSSION

For the numerical study, a four bladed soft-inplane hingeless rotor is considered. The rotor properties are given in Table 1. The baseline blade has zero chordwise offsets of blade center of gravity, aerodynamic center and tensile axis from the elastic axis ($y_0 = e_d = e_A = 0$). The aerodynamic center is assumed fixed at the quarter chord. The baseline blade is rectangular ($\Lambda_1 = \Lambda_2 = c_{tp} = c_0$). The fuselage center of gravity lies on the shaft axis ($X_{cg} = Y_{cg} = 0$) at a distance of $0.2R$ below the rotor hub center. For the analysis, the blade is divided into five equally spaced finite elements. For discretization in the time domain, four temporal finite elements with quartic polynomial distribution within each element are used. A stability analysis is performed in the rotating frame using the Floquet Transition matrix theory, and the fourth order Runge Kutta method is used for calculating the transition matrix and its derivatives. Eight normal modes (three flap, two lag, two torsion and one axial) are used for the trim analysis, and seven modes (three flap, two lag and two torsion) are used for the stability analysis. Results are obtained at a forward speed of $\mu = 0.3$ and a C_T of 0.0049.

The blade spar is made of Graphite/Epoxy (AS4/3501-6) plies, the properties of which are shown in Table 2. Optimization results are obtained for a two-cell composite box-beam, the dimensions of which are shown in Fig. 1. Each wall of the box-beam has 26 plies. By choosing different ply layups, selected couplings can be introduced. The configuration consisting of balanced laminates with no elastic couplings is designated as Uncoupled A (Table 3). Ply orientation angles used in defining the layups are positive towards the leading edge for the horizontal spar walls (top and bottom) and positive towards the bottom for the vertical spar walls. The Uncoupled A configuration is used as a starting point in this study. Flapwise bending-torsion coupling (pitch-flap coupling) can be introduced in this layup by unbalancing the top and bottom walls of the beam. Chordwise bending-torsion coupling (pitch-lag coupling) can be introduced by unbalancing the side walls of the beam. The Symmetric A layup (Table 3) exhibits pitch-flap couplings and Symmetric D layup displays pitch-lag couplings respectively. The signs of the coupling depend on the values of the angles θ_1, θ_2 and θ_3.

The optimization study uses the ply angles of the walls of the two-cell box-beam as well as blade sweep, droop, planform taper and tuning masses as the design variables. Typically, ply angles influence both elastic stiffnesses and elastic couplings. To filter the effect of elastic coupling on the optimum design, optimization is performed for both uncoupled and coupled layups. The uncoupled optimum reflects the influence of elastic stiffness only and is used as a baseline design with which the coupled optimum designs are compared.

Table 1-Rotor Properties

Number of Blades	4
Radius, ft	16.2
Hover Tip Speed,ft/s	650
c_0, c_1	0.0, 5.73
d_0, d_1, d_2	0.0095,0.0,0.2
c_m	0.0
c/R	0.055
Solidity, σ	0.07
Precone β_p	0.0
Lock Number, γ	6.34

The composite design variables are θ_1^i, θ_2^i and θ_3^i where i represents the ith spatial finite element (see Table 3). At each element location, these design variables affect 12 plies in each wall and hence results in a total of 60 plies for the five walls of the two-cell box-beam. Each wall consists of 26 plies which totals to 130 plies for the box-beam. The 0^o and 45^o plies are unchanged to assure that the optimum design does not become unrealistic. In this way, implicit move limits are imposed on the values of the elastic stiffnesses. Therefore, at each spanwise element, the ply angles of 12 plies undergo change during the optimization process while the remaining 14 plies undergo no change.

Table 2-Composite Spar Properties

Longitudinal modulus E_L, msi	20.59
Transverse Modulus E_T,msi	1.42
Shear Modulus G_{LT}, msi	0.87
Major Poisson Ratio ν_{LT}	0.42
Outer box width, in	4.2
Outer box depth, in	2.2
Number of plies in each wall	26
Ply thickness, in	0.005

The optimization is performed to minimize the objective function J defined by Eq. 7. For the optimization results, constraints are imposed on blade frequency, stability and autorotational inertia. Move limits are also imposed on the design variables to keep the design realistic and improve convergence characteristics (shown in Table 4). The upper and lower bounds on the allowable frequencies are

$$0.60/rev \leq \omega_{1L} \leq 0.80/rev$$
$$1.08/rev \leq \omega_{1F} \leq 1.18/rev$$
$$2.50/rev \leq \omega_{1T} \leq 6.50/rev$$

For the autorotation constraint, a minimum value of R_a (ratio of blade inertia to baseline inertia) of 0.90 is chosen. This means that the blade moment of inertia in not allowed to become less than 90 percent of the baseline value. For the stability constraint, ϵ_k is chosen to be zero. This implies that

the rotor is assumed to become unstable only when the damping of any of the blade modes becomes negative.

To investigate the effects of the design variables on the objective function, the following four cases are chosen.

Case 1 (composite only) : θ_i

Case 2 (blade geometry only) : Λ_1, Λ_2, c_{tp}

Case 3 (composite and blade geometry) : θ_i, Λ_1, Λ_2, c_{tp}

Case 4 (composite, blade geometry and inertia) : θ_i, Λ_1, Λ_2, c_{tp}, m_{ns}, y_{ns}

For Case 1, design variables are the ply angles of the walls of the two-cell box-beam blade. These design variables (θ_1, θ_2 and θ_3) are considered at five spanwise stations along the blade, resulting in a total of fifteen design variables. For Case 2, design variables are sweep, droop and planform taper at five spanwise stations along the blade, resulting in a total of fifteen design variables. For Case 3, design variables include ply angles as well as sweep, droop and planform taper at five spanwise stations, resulting in a total of thirty design variables. Case 4 includes all design variables: ply angles, sweep, droop, planform-taper, and nonstructural mass and its offset from the elastic axis. This results in a total of forty design variables. For Case 1, Case 3 and Case 4, optimization is performed for three different layups as shown in Table 3. The Uncoupled A layup has no elastic coupling and the Symmetric A and Symmetric D layups have pitch-flap (flap bending-torsion) and pitch-lag (lag bending-torsion) coupling, respectively. The ply angles θ are allowed complete freedom to move in the design space; the optimizer can therefore select the desired sign of the coupling at any spanwise station. For Case 2 (blade geometry only), the Uncoupled A layup is used with the ply angles held fixed at $\theta_1 = 15^o$, $\theta_2 = 30^o$ and $\theta_3 = 15^o$.

Table 3-Layups for Optimization Study

	Uncoupled A
TOP	$[0_3/(\theta_1/-\theta_1)/(\theta_2/-\theta_2)/(\theta_3/-\theta_3)/(45/-45)_2]_s$
BOT	$[0_3/(\theta_1/-\theta_1)/(\theta_2/-\theta_2)/(\theta_3/-\theta_3)/(45/-45)_2]_s$
LFT	$[0_3/(\theta_1/-\theta_1)/(\theta_2/-\theta_2)/(\theta_3/-\theta_3)/(45/-45)_2]_s$
RHT	$[0_3/(\theta_1/-\theta_1)/(\theta_2/-\theta_2)/(\theta_3/-\theta_3)/(45/-45)_2]_s$
WEB	$[0_3/(\theta_1/-\theta_1)/(\theta_2/-\theta_2)/(\theta_3/-\theta_3)/(45/-45)_2]_s$
	Symmetric A
TOP	$[0_3/(\theta_1/\theta_1)/(\theta_2/\theta_2)/(\theta_3/\theta_3)/(45/-45)_2]_s$
BOT	$[0_3/(\theta_1/\theta_1)/(\theta_2/\theta_2)/(\theta_3/\theta_3)/(45/-45)_2]_s$
LFT	$[0_3/(\theta_1/-\theta_1)/(\theta_2/-\theta_2)/(\theta_3/-\theta_3)/(45/-45)_2]_s$
RHT	$[0_3/(\theta_1/-\theta_1)/(\theta_2/-\theta_2)/(\theta_3/-\theta_3)/(45/-45)_2]_s$
WEB	$[0_3/(\theta_1/-\theta_1)/(\theta_2/-\theta_2)/(\theta_3/-\theta_3)/(45/-45)_2]_s$
	Symmetric D
TOP	$[0_3/(\theta_1/-\theta_1)/(\theta_2/-\theta_2)/(\theta_3/-\theta_3)/(45/-45)_2]_s$
BOT	$[0_3/(\theta_1/-\theta_1)/(\theta_2/-\theta_2)/(\theta_3/-\theta_3)/(45/-45)_2]_s$
LFT	$[0_3/(-\theta_1/-\theta_1)/(-\theta_2/-\theta_2)/(-\theta_3/-\theta_3)/(45/-45)_2]_s$
RHT	$[0_3/(-\theta_1/-\theta_1)/(-\theta_2/-\theta_2)/(-\theta_3/-\theta_3)/(45/-45)_2]_s$
WEB	$[0_3/(\theta_1/-\theta_1)/(\theta_2/-\theta_2)/(\theta_3/-\theta_3)/(45/-45)_2]_s$

Before proceeding with the optimization study, it should be noted that the first six harmonics of the flap and lag bending moments are used to calculate the component J_d (Eq. 6)in the objective function J. It is found that these harmonics are sufficient to represent the vibratory bending moments; the torsional moment is an order of magnitude smaller than the flap and lag bending moments.

Table 4. Bounds on Design Variables

Design Variable	Lower Bound	Upper Bound
θ_i	-90^0	90^0
Λ_1	-35^0	35^0
Λ_2	-20^0	20^0
c_{tp}/c	0.60	1.40

Optimization of a Composite Rotor (Case 1)

For Case 1, optimization is performed for the Uncoupled A layup. For this case, the blade geometry is held fixed at the baseline value. For the starting design, the design variables are $\theta_1 = 15^o$, $\theta_2 = 30^o$ and $\theta_3 = 15^o$. This starting design (called Starting Design A) is feasible and the optimizer shows good convergence characteristics when starting from this design. All optimization cases in this paper are started from Starting Design A. There is a reduction in the objective function J of 18 percent, with adjustments of direct stiffnesses of the blade (see Table 5). Next, the optimization is conducted for the Symmetric A (pitch-flap coupled) and Symmetric D (pitch-lag coupled) layups. Compared to the Uncoupled A optimum design, there is a further reduction in J of 16 percent for the Symmetric A design and of 3 percent for the Symmetric D design. As expected, pitch-lag coupling has negligible influence on vibratory hub loads and blade bending moments.

For the Symmetric A optimum design, there is a reduction in all six 4/rev hub loads, compared to Starting Design A. The magnitude of the 4/rev longitudinal, lateral and vertical forces are reduced by 20, 15 and 20 percent, respectively, and the 4/rev rolling, pitching and yawing moments are reduced by about 30, 30 and 60 percent, respectively (Fig. 2). The peak-to-peak flap and lag bending moments are reduced by 11 percent and 14 percent, as shown in Fig. 3. The above results show that by using elastic stiffness and pitch-flap coupling, it is possible to reduce both the vibratory hub loads and the vibratory bending moments. However, this reduction comes at the expense of lag mode stability; the lag mode damping is reduced by over 50 percent, from the Starting Design A value as shown in Fig. 4. The dampings of highly damped flap and torsion modes, are increased by 5 percent and 30 percent, respectively.

Table 5. Objective Function Normalized by Starting Design

Cases	J
Starting Design	1.00
Case 1 (Uncoupled A)	0.82
Case 1 (Symmetric A)	0.66
Case 1 (Symmetric D)	0.79
Case 1 (Symmetric D, infeasible starting design)	1.09
Case 2 (Advanced Geometry, Starting Design)	0.77
Case 3 (Uncoupled A)	0.62
Case 3 (Symmetric A)	0.52
Case 3 (Symmetric D)	0.58
Case 4 (Uncoupled A)	0.57
Case 4 (Symmetric A)	0.46
Case 4 (Symmetric D)	0.54

For the Uncoupled A optimum design, the flap and lag stiffness are reduced at the root element by 15 percent each and increased at the four outboard elements, compared to the starting design (Fig. 5(a) and 5(b)). The torsion stiffness shown in Fig. 5(c) is reduced throughout the blade span, the maximum reduction occuring at the second and third elements (about 30 percent). The Symmetric A optimum design shows similar results for the flap and lag stiffness, however, the torsion stiffness is increased at the inboard elements by about 10 percent and reduced at the outboard elements. The distribution of pitch-flap coupling for the optimum design in Fig. 6 shows the largest coupling at the two inboard and tip elements and lesser coupling at other elements. Again, the coupling is positive in sign throughout the blade.

The above results showed that elastic stiffness and pitch-flap coupling can be tailored to reduce vibratory hub loads and bending moments. However, pitch-lag coupling was found to have negligible effect on the optimum designs. It is well known that pitch-lag coupling has beneficial effects on aeroelastic stability, and since the stability constraint did not become active for the results shown above, pitch-lag coupling was not fully exploited.

To make the stability constraint active during the optimization process, a margin of 3 percent damping is imposed on the lag mode damping. This makes the Starting Design A an infeasible design

($\sigma_L = 0.0099 < 0.03$). The optimization is then performed for the Uncoupled A, Symmetric A and Symmetric D layups.

The Uncoupled A and Symmetric A layups are unable to satisfy the 3 percent requirement on lag mode damping. Only the Symmetric D layup (pitch-lag coupling) reaches an optimum design in the feasible region. For comparison, the Uncoupled A design obtained earlier for Case 3 with zero stability margin on lag mode damping is used as a baseline design. There is an increase in the lag mode damping of about 200 percent for the Symmetric D design, compared to the Uncoupled A design. This increase in lag mode damping comes at the expense of an increase in the objective function J of about 10 percent. This increase in the objective function is due to an increase in both the vibratory hub loads and the vibratory bending moments, as shown in Fig. 2 and 3, respectively. The elastic stiffness and coupling for the optimum design is shown in Figs. 5 and 6, respectively. The pitch-lag coupling ($\bar{k}_{24}$) is negative and is distributed quite evenly along the blade span.

The ply angle design variables corresponding to the starting and optimum designs are shown in Fig. 7. The optimum angles are obtained by rounding-off the optimum design to the nearest integer value. Results shown in this paper are obtained by performing the aeroelastic analysis with these integer ply angles. Laminates with such integer ply angles can be fabricated using automated composite fabrication techniques. Also, it was found that the optimum designs are robust, which means that small changes in the ply angles do not cause large changes in the objective function. Therefore, small errors during manufacturing such laminates may not cause a large change in the optimum design. Most of the ply angle design variables have values between 0 and 30 degrees. This may be because elastic couplings are largest between these angles.

Thus, using elastic stiffness and pitch-lag coupling yields a reduction in the vibratory hub loads and bending moments and an increase in the lag mode damping compared to the Starting Design A.

Optimization of Advanced Geometry Rotor (Case 2)

Next, the optimization is performed for Case 2 for which design variables are sweep, droop and planform taper along the blade span. Ply angles are held fixed for this case at values corresponding to Starting Design A. There is a reduction in the objective function J of 23 percent compared to the baseline value. A further reduction in J is not possible due to the lag mode damping becoming zero. This reduction in vibratory loads is due to blade geometry only. There is a general reduction in all the 4/rev hub loads compared to the baseline design (Fig. 2). The 4/rev longitudinal, lateral and vertical forces are reduced by 15, 20 and 25 percent, respectively, and the rolling, pitching and yawing moments are reduced by 20, 30 and 50 percent, respectively. The peak-to-peak flap and lag bending moments are reduced by about 10 percent each. The stability results in Fig. 4 shows that there is a reduction in the flap, lag and torsion mode damping for the Case 2 design, compared to the baseline design. In fact, the lag mode damping becomes active at the optimum point.

The spanwise variation of sweep, droop and planform taper for the optimum design is shown in Fig. 8(a), 8(b) and 8(c), respectively. The optimum design is tapered at the outer 60 percent of the blade span (taper ratio = 1.57). The inboard two elements show very small change in chord length. The optimum design is swept-back and drooped downwards over the entire blade span. The distribution of sweep, droop and planform taper show that outboard sections are more important for these design variables than inboard ones. This may be because at the outboard sections, the dynamic pressure is higher and the advanced geometry design variables depend on dynamic pressure for their effectiveness in load reduction. The reduction in the vibratory loads due to sweep and droop may be caused by beneficial coupling between the modes of deformation introduced by sweep and droop as well as by alleviation of compressibility effects at the blade tips due to sweepback. The planform taper distribution helps to shift the load distribution more towards the root end of the blade, thereby unloading the tip sections.

Optimization of Advanced Geometry Composite Rotor (Case 3)

For Case 3, both ply angles and advanced geometry design variables are used. For all Case 3 results, optimization is started from the Case 2 optimum design; this design has sweep, droop and planform taper but ply angles are fixed at the Starting Design A. Optimization is first performed for the Uncoupled A layup. Compared to Starting Design A, there is a reduction in the objective function of 38 percent, then the stability constraint becomes active due to the lag mode damping becoming zero. For Case 1,

the reduction in J is for the Uncoupled A layup is 18 percent and for Case 2, the reduction in J due to blade geometry alone is 23 percent. Using elastic stiffness and blade geometry together results in a payoff since J is reduced by 38 percent for the Case 3 optimum design.

Next, optimization is performed for the Symmetric A layup. For the Symmetric A layup, a 48 percent reduction is obtained in the objective function, compared to Starting Design A; at this point the stability constraint becomes active due to the lag mode damping going to zero. For Case 1, the reduction in J of 34 percent is obtained for the Symmetric A layup, compared to the starting design. Using blade advanced geometry variables therefore results in an additional reduction of 14 percent, compared to when only ply angle design variables are used. For the optimum design, the 4/rev longitudinal, lateral and vertical forces are reduced by about 30, 30 and 40 percent respectively, and the rolling, pitching and yawing moments are reduced by 40, 40 and 60 percent, respectively (Fig. 2). The peak-to-peak flap and lag bending moments are reduced by 14 and 18 percent, respectively, as shown in Fig. 3.

The flap, lag and torsion stiffness for the Symmetric A optimum design are shown in Fig. 5(a), 5(b) and 5(c), respectively. The flap and lag stiffnesses are reduced at the root element and increased throughout the rest of the blade. The torsion stiffness is reduced at element 3, at other elements it remains almost at the starting values. Positive pitch-flap coupling is distributed almost uniformly throughout the blade length. The blade has sweep and droop along the blade span, as shown in Fig. 8(a) and 8(b), respectively. The optimum design is tapered (taper ratio = 1.42) at the outer 60 percent of the blade span, as shown in Fig. 8(c). While the distribution of sweep and droop is similar to Case 2, the magnitude is lesser.

Next, optimization is performed for the Symmetric D layup. The objective function is reduced by about 42 percent, compared to the Starting Design A. At this point, the lag mode damping becomes very close to zero, as shown in Fig. 4. For this optimum design, the 4/rev longitudinal, lateral and vertical forces are reduced by about 30, 40 and 30 percent, respectively, and the 4/rev rolling, pitching and yawing moments are reduced by about 40, 40 and 50 percent, respectively (Fig. 2). Also, the peak-to-peak value of the flap and lag bending moments are reduced by 12 and 17 percent, respectively, as shown in Fig. 3.

The flap, lag and torsion stiffness for the Symmetric D optimum design are shown in Fig. 5(a), 5(b) and 5(c), respectively. The flap and lag stiffness are reduced at the root element and increased throughout the rest of the blade. The torsion stiffness is reduced at element 3, at other elements it remains almost unchanged from the starting value. The variation of pitch-lag coupling along the blade span is shown in Fig. 6. The pitch-lag coupling is negative and distributed throughout the blade span; the largest coupling occurs at the root element and at the two outboard elements. The spanwise distribution of sweep, droop and planform taper for the Case 3 optimum design is shown in Figs. 8(a), 8(b) and 8(c), respectively. The optimum design is tapered at the outer 80 percent of the blade span (taper ratio = 1.89). The distribution of sweep and droop along the span is similar to Case 2; the blade is swept back and drooped downwards throughout the blade span. However, the magnitude of the sweep and droop is considerably more compared to Case 2 as well as Case 3 (Symmetric A). The extra sweep and droop results in a greater reduction in the objective function compared to Case 2 and the destabilizing effects of this large sweepback is prevented by the negative pitch-lag coupling.

Optimization of an Advanced Geometry Rotor with Inertial Design Variables (Case 4)

Finally, results are obtained for Case 4, which includes all design variables (ply angles, sweep, droop, planform taper and nonstructural mass and its chordwise offset from the elastic axis). For all Case 4 results, the optimization is started from the Case 2 optimum design. The optimization is first performed for the Uncoupled A layup. There is a reduction in the objective function of 43 percent compared to Starting Design A, after which any further reduction is prevented because the lag mode becomes unstable. For Case 1, Case 2 and Case 3, the reduction of J for the Uncoupled A layup was 18, 23 and 38 percent, respectively. The inertia design variables therefore cause an additional reduction in the objective function of about 5 percent, when compared to Case 3(blade geometry and composite).

Next, optimization is performed for the Symmetric A layup. For the Symmetric A layup, there is a reduction in the objective function J of 54 percent compared to the starting design. Further reduction in J is prevented because the lag mode becomes unstable. For the optimum design, the 4/rev longitudinal, lateral and vertical forces are reduced by about 45, 40 and 45 percent and the 4/rev rolling, pitching and yawing moments are reduced by 50, 50 and 60 percent. The peak-to-peak flap and lag moments are

reduced by 17 and 26 percent, respectively. The distribution of elastic stiffness and pitch-flap coupling for the optimum design is similar to Case 3 (Symmetric A) design (Fig. 5 and 6). The optimum design is swept back and drooped down along the blade length, however, the magnitude of sweep and droop is less that in Case 3. The blade is tapered along the outer 60 percent, with a taper ratio of 1.34. The nonstructural mass is placed aft of the elastic axis for the outboard three elements, as shown in Fig. 9(a) and 9(b), respectively. The nonstructural mass increases the inertial force as well as the stiffening centrifugal force. At the blade tip, the centrifugal stiffening forces become much larger than the inertial forces leading to a decrease in the 4/rev loads. The nonstructural mass also causes a shift in the blade cg, which leads to couplings between the flap and torsion modes of deformation. The ply angle design variables corresponding to the optimum design are shown in Fig. 7. These angles are similar to those obtained for Case 3.

Next, optimization is performed for the Symmetric D layup. There is a reduction in the objective function of about 46 percent before the lag mode becomes unstable. For this optimum design, the 4/rev longitudinal, lateral and vertical forces are reduced by about 40 percent each, the 4/rev rolling, pitching and yawing moments are reduced by about 40, 45 and 60 percent (Fig. 2) and the vibratory flap and lag bending moments are reduced by about 10 and 17 percent (Fig. 3). The reduction in loads comes as the expense of lag mode stability; the stability constraint for lag mode damping is active at the optimum design (Fig. 4).

The distribution of sweep, droop and planform taper is shown in Fig. 8. The blade is swept back and drooped down along the entire length, as in Case 2 and Case 3, and has a taper ratio of 1.89. However, the tip element has less sweepback and droop than the Case 3 Symmetric D design. This may be because the use of nonstructural mass as design variables in Case 4 (Symmetric D) requires less sweepback to achieve a reduction in the objective function. The spanwise distribution of nonstructural mass and the offset of nonstructural mass from the elastic axis are shown in Figs. 9(a) and 9(b), respectively for the Case 4 optimum designs. For the Case 4 optimum design the nonstructural masses are placed aft of the elastic axis for the outboard three elements. The elastic stiffnesses, pitch-lag coupling and ply angles for the Case 4 (Symmetric D) design are similar to the Case 3 (Symmetric D) design

The optimum designs for the cases discussed above are compared at the same thrust condition ($C_T = 0.0049$). The C_T/σ value for Case 1 is unchanged from the baseline value of 0.07. For Case 2, Case 3(Symmetric A), Case 3(Symmetric D), Case 4(Symmetric A) and Case 4(Symmetric D) the solidity of the blade is changed and the value of C_T/σ are 0.086, 0.078, 0.108, 0.073 and 0.104 respectively. All the results obtained above are obtained for an advance ratio of $\mu = 0.3$. To see if the optimum designs are effective at off-design conditions, the objective function J is shown with advance ratio varying from 0 to 0.4 in Fig. 10. It can be observed that there is a reduction in the objective function at all advance ratios. In fact, the reduction in J is larger at higher advance ratios.

4. CONCLUSIONS

Using an analytical formulation, rotor aeroelastic and sensitivity analysis are developed for an advanced geometry composite blade with a generic spar. For the numerical results, a four-bladed soft-inplane hingeless rotor is investigated. The composite blade is modeled as a two-cell box-beam. Design variables are the ply angles of the laminated walls of the composite box-beam as well as blade sweep, droop, planform-taper, and nonstructural mass and its offset from the elastic axis. The study is divided into four parts:

Composite Rotor Optimization

1. Using only ply angles as deign variables for the Uncoupled A layup, the objective function J is reduced by 18 percent from the starting design. The Symmetric A (pitch-flap coupled) layup shows a further reduction of 16 percent; the 4/rev loads are reduced by 20-60 percent compared to the starting design and the peak-to-peak flap and lag bending moments are reduced by 11 and 14 percent, respectively. However, the lag mode damping is reduced by 50 percent.

2. Starting from an initially infeasible design with a damping margin of 3 percent in the lag mode, the Symmetric D layup (pitch-lag coupled) resulted in an increase in the lag mode damping of over 200 percent compared to the optimum solution for the Uncoupled A blade. This increase in lag damping comes at the expense of an increase in the objective function of 9 percent.

Advanced Geometry Rotor Optimization

3. Using only spanwise variation of blade sweep, droop and planform taper as design variables, the objective function J is reduced by 23 percent from the starting design. Further reduction in the objective function is prevented because of the lag mode damping becoming zero. The 4/rev loads are reduced by 15-50 percent and the peak-to-peak flap and lag bending moments by about 10 percent each. The reduction in loads due to sweep and droop may be caused by beneficial coupling between the modes of deformation and by alleviation of compressibility effects at the blade tips.

4. The optimum design is swept-back and drooped-downwards along the blade span and has a taper ratio of 1.57.

Advanced Geometry Composite Rotor Optimization

5. Using blade geometry design variables (Case 3) and ply angle design variables for the Uncoupled A layup, the objective function J is reduced by 38 percent compared to the starting design; at this point the lag damping becomes zero. The Symmetric A layup (pitch-flap coupled) leads to a reduction of 48 percent from the starting design before the lag mode becomes unstable; the 4/rev loads are reduced by 30-60 percent and the peak-to-peak flap and lag bending moments by about 14 and 18 percent, respectively

6. The Symmetric D layup (pitch-lag coupled), shows a reduction in the objective function of 42 percent from the starting design; the 4/rev loads are reduced by 40-60 percent and the peak-to-peak vibratory flap and lag bending moments by about 12 and 17 percent, respectively.

Advanced Geometry Composite Rotor Optimization with Inertial Distribution

7. Using all design variables for the Uncoupled A layup (Case 4), the objective function J is reduced by 43 percent compared to the starting design; at this point the lag damping becomes zero. The Symmetric A layup (pitch-flap coupled) leads to a reduction of 54 percent from the starting design before the lag mode becomes unstable; the 4/rev loads are reduced by 40-60 percent and the peak-to-peak flap and lag bending moments by 17 and 26 percent.

8. The Symmetric D layup (pitch-lag coupled), shows a reduction in the objective function of 46 percent from the starting design; the 4/rev loads are reduced by 40-60 percent and the peak-to-peak vibratory flap and lag bending moments by about 10 and 17 percent, respectively.

9. Even though the optimization is performed at $\mu = 0.3$, reduction in both vibratory hub loads and bending moments are observed at all forward speeds. In fact, there is a larger reduction in both vibratory hub loads and bending moments at higher advanced ratios.

5. ACKNOWLEDGEMENT

This work is supported by the Army Research Office, Contract No. DAAH04-93-G-001. Technical monitors are Dr. Robert Singleton and Dr. Tom Doligalski.

REFERENCES

[1] Celi, R., and Friedmann, P.P., "Structural Optimization with Aeroelastic Constraints of Rotor Blades with Straight and Swept Tips," *AIAA Journal*, Vol. 28, No. 5, pp. 928-936.

[2] Ganguli,R., and Chopra, I., "Aeroelastic Optimization of an Advanced Geometry Helicopter Rotor", *Proceedings of the 33rd AIAA/ASME/ASCE/AHS/ASC Structures, Structural Dynamics and Materials Conference*, April 13-15,1992, Dallas, Texas.

[3] Celi, R., and Friedmann, P.P., "Aeroelastic Modeling of Swept Tip Rotor Blades Using Finite Elements," *Journal of the American Helicopter Society*, Vol. 33, No. 2, April 1988, pp. 43-52.

[4] Benquet, P., and Chopra, I., " Calculated Dynamic Response and Loads for an Advanced Tip Rotor in Forward Flight," Proceedings of the 15th European Rotorcraft Forum, Amsterdam, Netherland, Sep 1989.

[5] Kim, K.C., and Chopra, I., "Aeroelastic Analysis of Helicopter Blades w ith Advanced Tip Shapes," *Journal of the American Helicopter Society*, Vol. 37, No. 1, Jan 1992, pp. 15-30.

[6] Bir, G., Chopra, I., "Aeromechanical Stability of Rotorcraft with Advanced Geometry Blades," Presented at the AIAA 34the Structures, Structural Dynamics and Materials Conference, La Jolla, Calif, Apr 1993.

[7] Hong, C.H., and Chopra, I., "Aeroelastic Stability of a Composite Blade," *Journal of the American Helicopter Society*, Vol. 30, (2), 1985.

[8] Panda, B., and Chopra, I., "Dynamics of Composite Rotor Blades in Forward Flight," *Vertica*, Vol. 11, (1/2), 1987.

[9] Smith, E.C., and Chopra, I., "Aeroelastic Response, Loads and Stability of a Composite Rotor in Forward Flight," *AIAA Journal*, Vol. 31, (7), 1993, pp. 1265-1274.

[10] Fulton, M., and Hodges, D., "Applications of Composite Rotor Stability to Extension-Twist Coupled Blades," Proceedings of the 33rd AIAA/ASME/ASCE/AHS/ASC Structures, Structural Dynamics and Materials Con ference, AIAA Paper No. 92-2254, Dallas, Texas, Apr 13-15 1992.

[11] Yuan, I, Friedmann, P.P., and Venkatesan, C., "A New Aeroelastic Model for Composite Rotor Blades with Straight and Swept Tips," Proceedings of the 33rd AIAA/ASME/ASCE/AHS/ASC Structures, Structural Dynamics and Materials Con ference, AIAA Paper No. 92-2259, Dallas, Texas, Apr 13-15 1992.

[12] Smith, E.C., and Chopra, I., "Air and Ground Resonance of Helicopters with Elastically Tailored Composite Rotor Blades," *Journal of the American Helicopter Society*, Vol. 38, (4), October, 1993.

[13] Ganguli,R., and Chopra, I., "Aeroelastic Optimization of a Composite Helicopter Rotor," *Presented at the 4th AIAA/USAF/NASA/OAI Symposium on Multidisciplinary Analysis and Optimization*, September 21-23, 1992, Cleveland, Ohio

[14] Ganguli, R., and Chopra,I., " Aeroelastic Optimization of a Helicopter Rotor with Composite Tailoring," *Proceedings of the 49th Annual Forum and Technology Display of the American Helicopter Society*, May 19-21, 1993, St. Louis, Missouri.

[15] Ganguli, R., and Chopra, I., "Multi-Objective Optimization of a Composite Helicopter Rotor", *Proceedings of the 35th Structures, Structural Dynamics and Materials Conference and Adaptive Structures Forum*, Hilton Head, South Carolina, April 1994.

[16] Friedmann, P.P., "Helicopter Vibration Optimization using Structural Optimization with Aeroelastic/ Multidisciplinary Constraints," *Journal of Aircraft*, Vol. 28, No. 1, 1991, pp. 8-21.

[17] Davis, M.W., and Weller, W.H., "Helicopter Rotor Dynamics Optimization with Experimental Verification," *Journal of Aircraft*, Vol. 28, No. 1, 1991, pp. 38-48.

[18] Young, D.K., and Tarzanin Jr., F.J., " Structural Optimization and Mach Scale Test Validation of a Low Vibration Rotor," *Journal of the American Helicopter Society*, Vol. 38, No. 3, July 1993, pp. 83-92.

[19] Lim, J., and Chopra, I., "Aeroelastic Optimization of a Helicopter Rotor using an Efficient Sensitivity Analysis," *Journal of Aircraft*, Vol. 28, No. 1, 1991, pp. 29-37.

[20] Bir, G., Chopra, I., et al., "University of Maryland Advanced Rotorcraft Code Theory Manual," UM-AERO Report 94-18, July 1992.

[21] Vanderplatts, G.N., "CONMIN - A Fortran Program for Constrained Function Minimization," User's Guide, NASA TMX 62282, August, 1973.

[22] Smith, E.C., and Chopra, I., " Formulation and Evaluation of an Analytical Model for Composite Box Beams," *Journal of the American Helicopter Society*, July 1991.

[23] Schmit, L.A., "Approximation Concepts for Efficient Structural Analysis," NASA CR-2552, 1976.

[24] Vanderplatts, G.N., "Approximation Concepts for Numerical Airfoil Optimization," NASA TP-1370, March 1979.

[25] Ganguli, R., "Aeroelastic Optimization of Advanced Geometry and Composite Helicopter Rotors", Ph.D. Thesis.

[26] Yuan, I., Friedmann, P.P., and Venkatesan, C., " Aeroelastic Behavior of Composite Swept Rotor Blades with Swept Tips," Proceedings of the 48th Annual Forum of the American Helicopter Society, Jun 3-5, 1992, Washington, D.C., Vol. 2.

[27] Epps, Jeanette J., and Chandra Ramesh., "Experimental-Theoretical Study of the Effects of Tip Sweep on the Natural Frequencies of Rotating Composite Beams", *Proceedings of the 35th Structures, Structural Dynamics and Materials Conference and Adaptive Structures Forum*, Hilton Head, South Carolina, April 1994.

[28] Chandra, R., and Chopra, I., " Structural Behavior of Two-Cell Composite Rotor Blades with Elastic Couplings", *AIAA Journal* , Vol. 30, No. 12, 1992, pp. 2914-2924.

[29] Gjelsvik, A., *The Theory of Thin Walled Bars*, John Wiley and Sons, 1981.

[30] Bir, Gunjit., and Chopra, Inderjit., " Status of University of Maryland Advanced Rotorcraft Code (UMARC)", Presented at the American Helicopter Society Aeromechanics Specialists Conference, San Francisco, California.

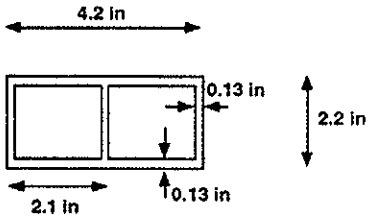

Fig. 1. Cross-sectional dimensions for the two-cell box-beam

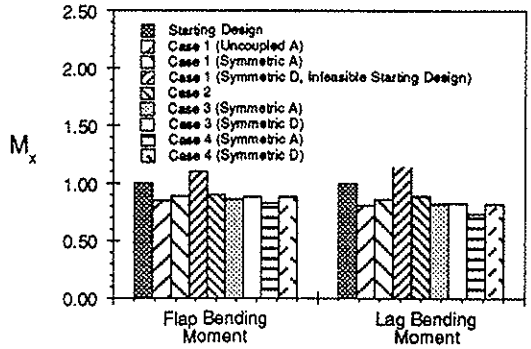

Fig. 3. Peak-to-Peak Bending Moments at Blade Root Normalized with Starting Design Values, Corresponding to Initial and Optimum Designs

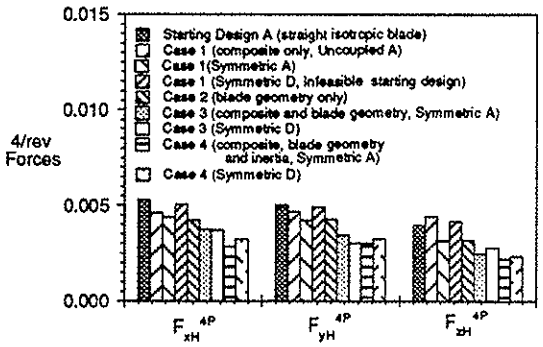

Fig. 2(a). Vibratory Hub Forces Corresponding to Initial and Optimum Designs

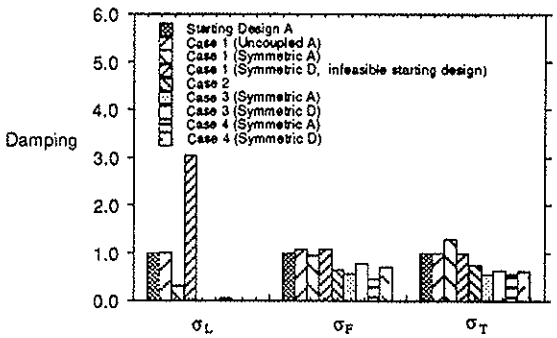

Fig. 4. Blade Damping Corresponding to the Initial and Optimum Designs

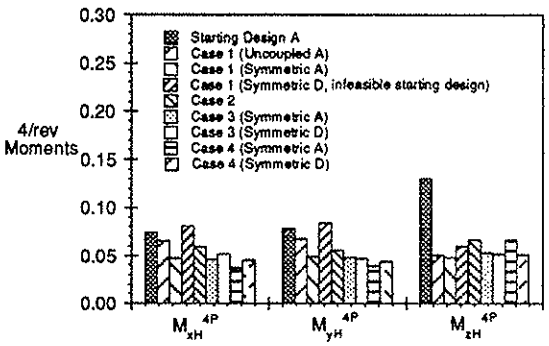

Fig. 2(b). Vibratory Hub Moments Corresponding to Initial and Optimum Designs

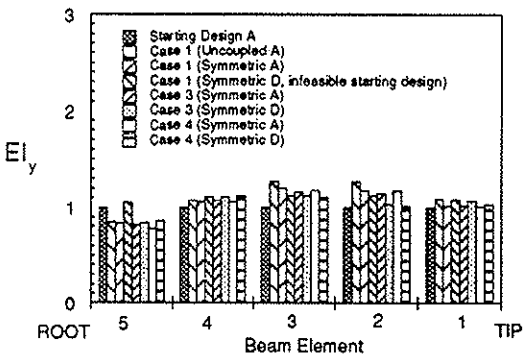

Fig. 5(a) Spanwise Distribution of Flap Stiffness, Normalized with Starting Design A values

Figure 1:

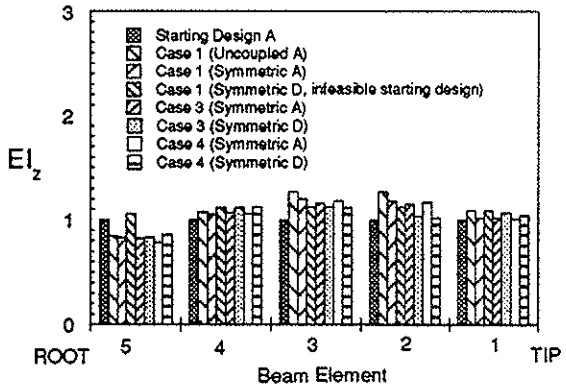

Fig. 5(b) Spanwise Distribution of Lag Stiffness, Normalized with Starting Design A values

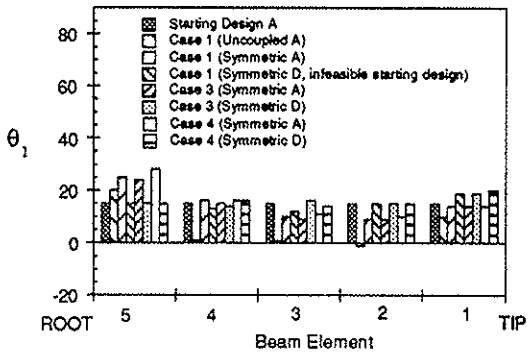

Fig. 7(a) Spanwise Distribution of Design Variable θ_1

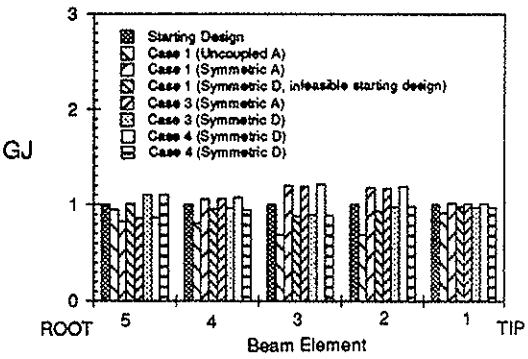

Fig. 5(c) Spanwise Distribution of Torsion Stiffness, Normalized with Starting Design A values

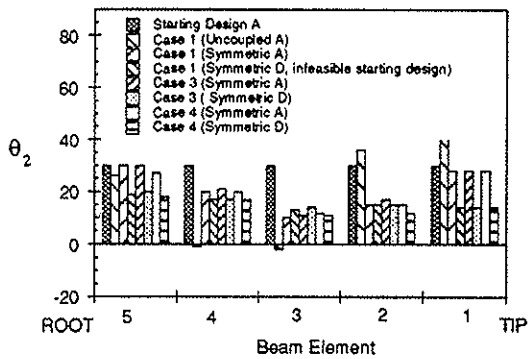

Fig. 7(b) Spanwise Distribution of Design Variable θ_2

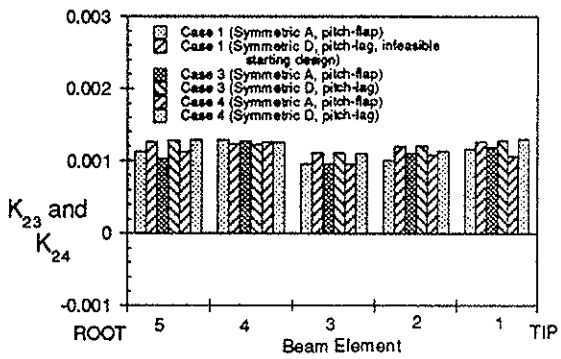

Fig. 6 Spanwise Distribution of Bending-Torsion Coupling for Coupled Optimum Designs

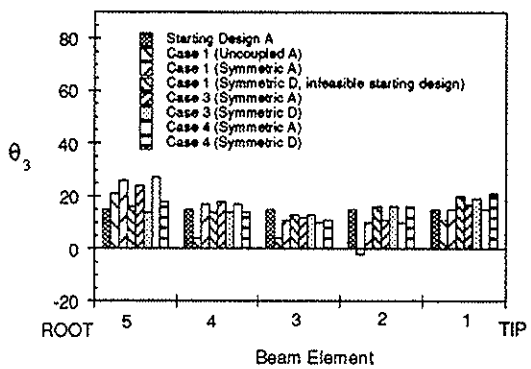

Fig. 7(c) Spanwise Distribution of Design Variable θ_3

Figure 2:

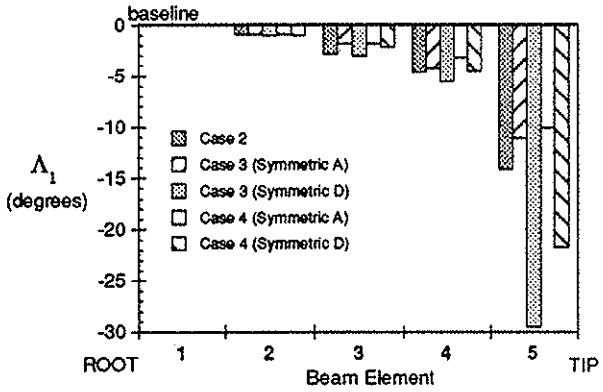

Fig. 8(a) Spanwise distribution of sweep for the optimum designs (negative sweep is backward)

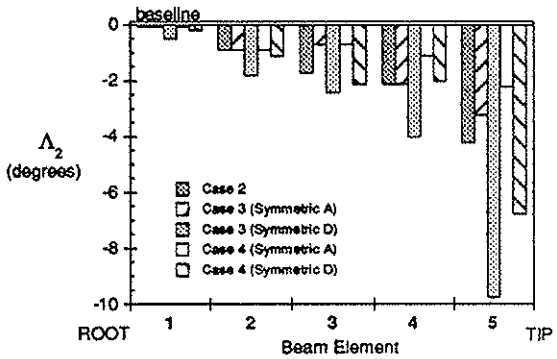

Fig. 8(b) Spanwise distribution of droop for the optimum designs (negative droop is downward)

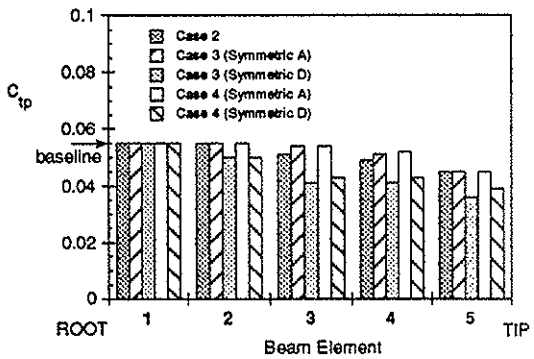

Fig. 8(c). Spanwise Distribution of Chord for the Optimum Designs

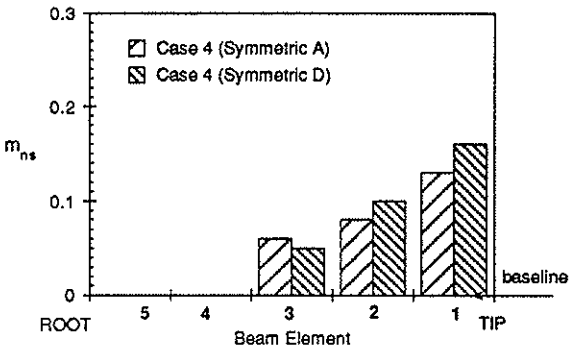

Fig. 9(a) Spanwise distribution of nonstructural mass for optimum designs

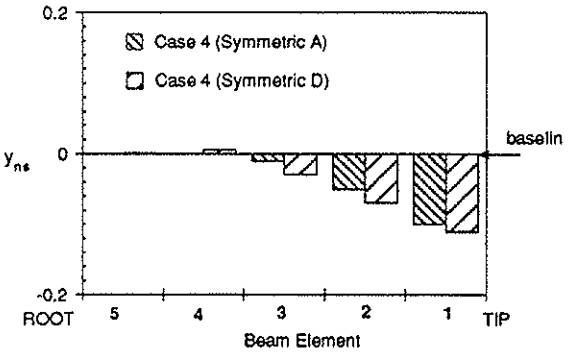

Fig. 9(b) Spanwise distribution of the offset of nonstructural mass from the elastic axis for optimum designs

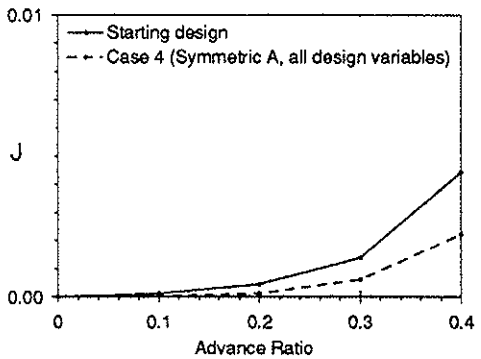

Fig. 10. The objective function for the Case 4 (Symmetric A) optim design at design (μ = 0.3) and off-design conditions

Figure 3: